

InsPose: Instance-Aware Networks for Single-Stage Multi-Person Pose Estimation

Dahu Shi
Hikvision Research Institute
Hangzhou, China
shidahu@hikvision.com

Wenming Tan
Hikvision Research Institute
Hangzhou, China
tanwenming@hikvision.com

Xing Wei
School of Software Engineering
Xi'an Jiaotong University
weixing@mail.xjtu.edu.cn

Ye Ren
Hikvision Research Institute
Hangzhou, China
renye@hikvision.com

Xiaodong Yu
Hikvision Research Institute
Hangzhou, China
yuxiaodong7@hikvision.com

Shiliang Pu*
Hikvision Research Institute
Hangzhou, China
pushiliang.hri@hikvision.com

ABSTRACT

Multi-person pose estimation is an attractive and challenging task. Existing methods are mostly based on two-stage frameworks, which include top-down and bottom-up methods. Two-stage methods either suffer from high computational redundancy for additional person detectors or they need to group keypoints heuristically after predicting all the instance-agnostic keypoints. The single-stage paradigm aims to simplify the multi-person pose estimation pipeline and receives a lot of attention. However, recent single-stage methods have the limitation of low performance due to the difficulty of regressing various full-body poses from a single feature vector. Different from previous solutions that involve complex heuristic designs, we present a simple yet effective solution by employing instance-aware dynamic networks. Specifically, we propose an instance-aware module to adaptively adjust (part of) the network parameters for each instance. Our solution can significantly increase the capacity and adaptive-ability of the network for recognizing various poses, while maintaining a compact end-to-end trainable pipeline. Extensive experiments on the MS-COCO dataset demonstrate that our method achieves significant improvement over existing single-stage methods, and makes a better balance of accuracy and efficiency compared to the state-of-the-art two-stage approaches.

KEYWORDS

Pose Estimation, Conditional Convolutions, Neural Networks

1 INTRODUCTION

Multi-person pose estimation aims to identify all the instances and detect the keypoints of each person simultaneously. It is a fundamental task and has a wide range of applications such as motion recognition [35, 37], person re-identification [20], pedestrian tracking [43], and athletic training assistance [36].

Multi-person pose estimation methods are usually based on two-stage frameworks including the bottom-up and top-down approaches. Bottom-up methods [3, 14, 25, 27, 28] first detect all the potential keypoints in the image in an instance-agnostic manner, and then perform a grouping process to get the final instance-aware poses. Usually, the grouping process is heuristic in which many tricks are involved and does not facilitate end-to-end learning. On

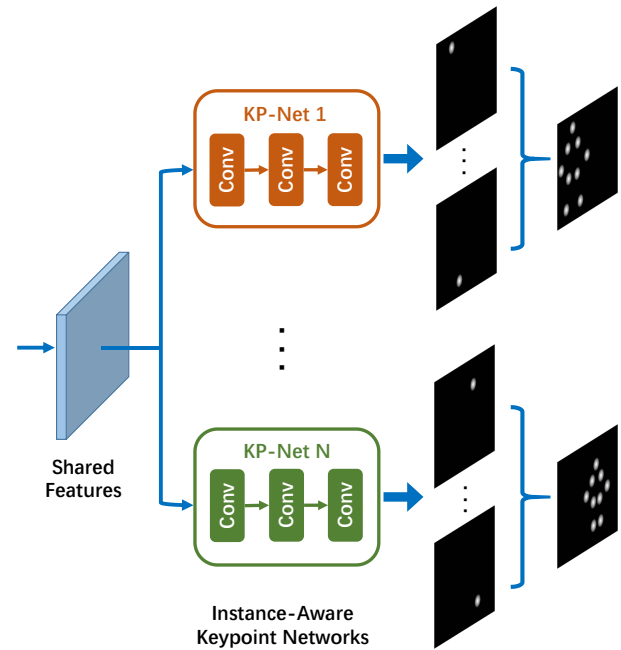


Figure 1: InsPose makes use of instance-aware keypoint networks (KP-Nets) to directly predict the full-body pose for each instance.

the other hand, top-down methods [1, 5, 7, 10, 11, 17, 32, 39] first detect each individual by a bounding-box and then transfer the task to an easier single-person pose estimation problem. While avoiding the heuristic grouping process, top-down methods come with the price of high computational complexity as mentioned in [26]. Especially, the running time of top-down methods depends on the number of instances contained in the image. Similarly, top-down methods are also not learned in an end-to-end fashion.

Recently, the single-stage pose estimation paradigm [26, 33, 38] is proposed and receives a lot of attention. This single-stage framework receives great interest since 1) it directly learns a mapping from the input image to the desired multi-person poses and is end-to-end trainable, and 2) it can consolidate object detection and

*Corresponding Author.

keypoint localization in a simple and unified framework, and thus 3) presents a more compact pipeline and attractive simplicity and efficiency over two-stage methods.

A straightforward way for single-stage pose estimation is adapting the bounding-box regression head of the single-stage object detectors [34, 41]. However, such a naive approach expects a single feature vector (namely, a point feature) to regress the precise locations of all the keypoints. While a point feature may be sufficient for bounding box regression to some extent, it is difficult to encode rich pose information considering that keypoints have much more geometric variations than the regular box corners. As a result, the pose estimation accuracy of this approach is unsatisfactory [33]. To deal with this problem, SPM [26] proposes a progressive joint representation by dividing body joints into hierarchies induced from articulated kinematics. CenterNet [42] proposes a hybrid solution by first regressing joint locations and then refining with the help of additional heatmaps. DirectPose [33] proposes a keypoint alignment module with the aim of aligning the point feature to the features around target joints. However, they all involve heuristic designs and still result in less accurate performance compared to the state-of-the-art bottom-up method [6], leaving room for further optimization.

In this paper, we present a direct and simple framework for single-stage multi-person pose estimation, termed *InsPose*. The core of our method is an instance-aware module to adaptively adjust (part of) the network parameters for each instance, as illustrated in Figure 1. Instead of using a standard keypoint network (called, KP-Nets) with fixed parameters for predicting all instances of various poses, we borrow the idea from recent dynamic neural networks [4, 9, 16, 40] to generate instance-aware parameters. Specifically, these KP-Nets are dynamically generated with respect to the different spatial locations of the input. Afterwards, they are applied to the whole feature maps to directly predict the full-body poses, get rid of the need for additional handcrafted processing. KP-Nets can better encode all kinds of pose variants since each one of them only focuses on an individual instance. Moreover, each KP-Net only consists of three 1×1 convolutions, leading to a compact and efficient architecture.

The overview of our method is illustrated in Figure 3 and we summarize our main contributions as below.

- We propose a simple single-stage network for multi-person pose estimation. It is end-to-end trainable and avoids many heuristic designs such as keypoints grouping [6], progressive pose representation [26], delicate feature aggregation [33], or pose anchors [38].
- The proposed model has a dynamic network that consists of instance-aware KP-Nets, which is different from previous methods that use a fixed set of convolutional filters for all the instances.
- We conduct extensive experiments on the COCO benchmark where our method outperforms state-of-the-art single-stage methods significantly and achieves a better trade-off between accuracy and efficiency compared to state-of-the-art two-stage approaches.

2 RELATED WORK

2.1 Multi-Person Pose Estimation

With the development of deep neural networks, modern pose estimation methods can be divided into three categories: top-down methods, bottom-up methods, and recent single-stage methods.

Top-down Methods. Top-down methods decouple the multi-person pose estimation task into two sub-tasks: multi-person detection and single-person pose estimation. The person detection is first performed to predict a bounding-box for each instance in the image. Then the instance is cropped from the bounding box for single-person pose estimation. Instead of cropping the original image, Mask RCNN [11] proposes to utilize extracted features to improve efficiency. A cascade pyramid network is proposed in CPN [5], aiming to regress difficult keypoints. Moreover, HRNet [32] focuses on learning reliable high-resolution representations and maintains high-resolution representations through the network. In general, top-down methods have better performance but also have higher computational complexity since they have to repeatedly perform single-person pose estimation for each instance. Moreover, top-down methods are highly dependent on the performance of the detectors.

Bottom-up Methods. On the other hand, bottom-up methods [3], [14], [25], [6] first detect all keypoints in instance-agnostic fashion. Then keypoints are assembled into full-body poses by a grouping process. Openpose [3] proposes to utilize part affinity fields to establish connections between keypoints of the same instance. Associative embedding [25] produces a detection heatmap and a tagging heatmap for each body joint, and then groups body joints with similar tags into individual people. Based on the above grouping strategy, HigherHRNet [6] proposes multi-resolution heatmap aggregation for more accurate human pose estimation. Bottom-up methods are usually more efficient because of their simpler pipeline of sharing convolutional computation. However, the grouping post-process is heuristic and involves many tricks which often makes its performance inferior to top-down methods.

Single-Stage Methods. Both top-down and bottom-up methods are not end-to-end trainable and have their own limitations. The single-stage methods [26], [42], [33], [38] are proposed recently to avoid the aforementioned difficulties. These methods predict instance-aware keypoints directly from estimated root locations [26], [42] or follow the dense predication strategy [38], [33] for estimating a full-body pose from each spatial location. SPM [26] proposes a structured pose representation to unify position information of person instances and body joints. DirectPose [33] and Point-set anchors [38] adopt deformable-like convolutions to refine the initial estimations, mitigating the difficulties of feature misalignment. The performance of DirectPose [33] is poor even with a well-designed feature aggregation mechanism. Although SPM and Point-set anchors achieve competitive performance among single-stage methods, they still fall behind the state-of-the-art bottom-up methods.

2.2 Dynamic Neural Networks

The dynamic neural network is an emerging research topic in deep learning. Unlike traditional neural networks which have a static model at the inference stage, dynamic networks can adapt their



Figure 2: Visualization results of the proposed InsPose on MS-COCO minival. InsPose can directly detect a wide range of poses, containing viewpoint change, occlusion, motion blur, multiple persons. Magenta, blue, and orange dots represent nose, keypoints of left body, and keypoints of right body, respectively. Note that some small-scale person do not have ground-truth keypoint annotations in the training set of MS-COCO, thus they might be missing when testing. Best viewed in color.

structures or parameters to different inputs, leading to advantages in terms of adaptiveness, capacity, efficiency, etc. A typical approach to parameter adaptation is adjusting the weights based on their input during inference. For example, conditionally parameterized convolution [40] and dynamic convolutional neural network [4] perform soft attention on multiple convolutional kernels to produce an adaptive ensemble of parameters without noticeably increasing the computational cost. On the other hand, weight prediction [9] directly generates (a subset of) instance-wise parameters with an independent model at test time. For instance, dynamic filter networks [16] build a generation network to predict weights for a convolutional layer.

In this work, we leverage this idea to produce instance-aware dynamic convolutional weights to solve the challenging multi-person pose estimation problem, as shown in Figure 2. In parallel to our work, Mao *et. al* [24] proposed a fully convolutional multi-person pose estimator. Our method and [24] both present a single-stage multi-person pose estimation framework using dynamic instance-aware convolutions, which achieve better accuracy/efficiency trade-off than other state-of-the-art methods.

3 APPROACH

In this section, we first introduce the overall architecture of our framework. Next, we elaborate on the proposed instance-aware dynamic network, which is capable of implementing the multi-person pose estimation task. Then we describe the disk offset prediction branch to reduce the discretization error. Finally, the loss function and the inference pipeline of our model are summarized.

3.1 Overview

Let $I \in \mathbb{R}^{H \times W \times 3}$ be an input image of height H and width W , multi-person pose estimation (a.k.a. keypoint detection) aims at estimating human poses \mathcal{P} of all the person instances in I . The ground-truths are defined as

$$\bar{\mathcal{P}} = \{P_i^1, P_i^2, \dots, P_i^K\}_{i=1}^N, \quad (1)$$

where N is the number of persons in the image, K is the number of keypoints (*i.e.*, left shoulder, right elbow), and $P_i^j = (x_i^j, y_i^j)$ denotes coordinates of the j th keypoint from the i th person.

Multi-Person Pose Representation. In this work, our core idea is that for an image with N instances, N different KP-Nets will be dynamically generated, and each KP-Net will contain the characteristics of the target instance in its filter kernels. As shown in Figure 1, when the KP-Net for person i is applied to an input, it will produce a keypoint map $M_i \in \mathbb{R}^{\frac{H}{s} \times \frac{W}{s} \times K}$, where s is the down-sampling ratio of the map. Then the maximal activation in j th channel of M_i (denoted as M_i^j) indicates the location of the j th keypoint for person i , which can be formulated as

$$\bar{P}_i^j = (\bar{x}_i^j, \bar{y}_i^j) = \arg \max_{x, y} M_i^j \quad (2)$$

To recover the discretization error caused by the down-sampling of keypoint maps, we additionally propose a disk offset prediction module. It predicts an instance-agnostic local offset $O \in \mathbb{R}^{\frac{H}{s} \times \frac{W}{s} \times 2K}$ for each category of keypoints. Then we pick the offset vector $(\Delta x, \Delta y)$ corresponding to the above keypoint location \bar{P}_i^j , the final keypoint location on the input image plane can be defined as

$$\hat{P}_i^j = \left((\bar{x}_i^j + \Delta x) \times s, (\bar{y}_i^j + \Delta y) \times s \right) \quad (3)$$

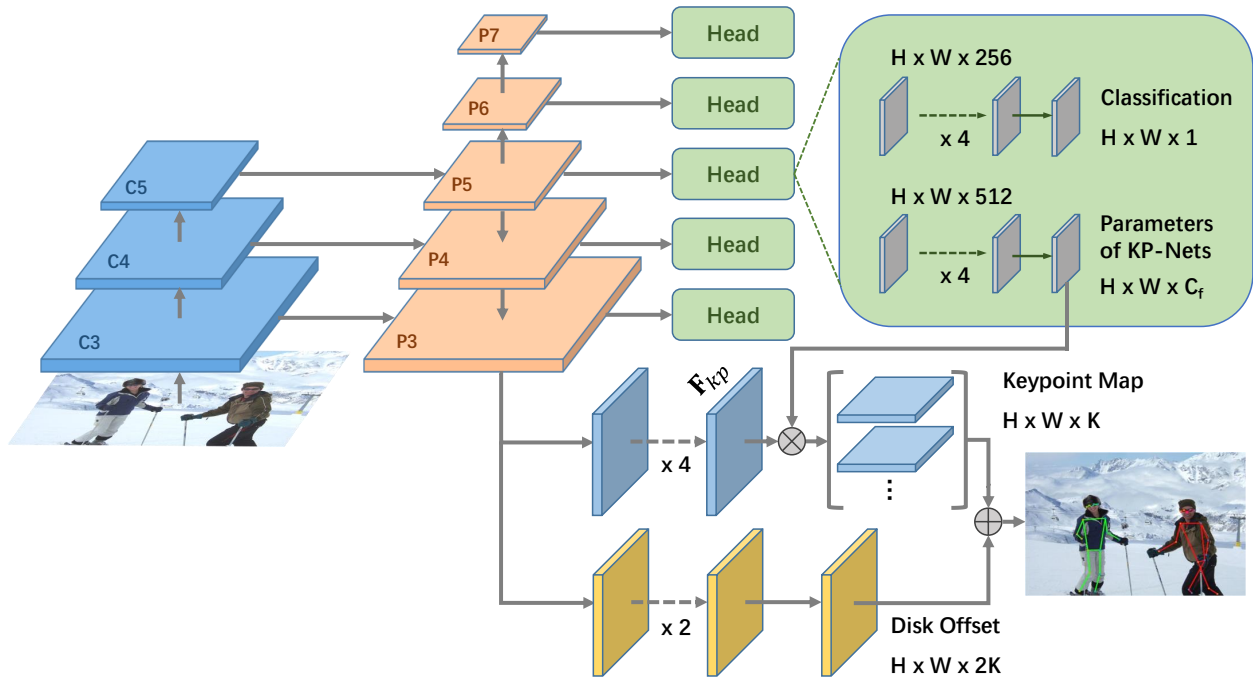


Figure 3: The overall architecture of InsPose. C_3, C_4, C_5 are the feature maps of the backbone network (e.g., ResNet-50). P_3 to P_7 are the FPN feature maps as in [21, 34], which are used for final predictions. $H \times W$ denotes the height and width of feature maps, and K is the number of keypoints for each instance. Classification head is used to classify the locations on the feature maps into "person" or "not person". The parameters of KP-Nets are dynamically generated with respect to different locations of the input. Then the learned parameters are split and reshaped as the weights and biases of convolutions in each KP-Net which is applied to predict keypoint maps for the particular instance. Disk offset branch predicts the instance-agnostic local offset to recover the discretization error caused by down-sampling.

Network Architecture. We build the proposed InsPose on the popular anchor-free object detector FCOS [34] due to its simplicity and flexibility, as shown in Figure 3. We make use of ResNet [13] or HRNet [32] as the backbone network. Then feature pyramid networks (FPN) [21] is employed to produce 5 feature pyramid levels $\{P_3, P_4, P_5, P_6, P_7\}$, whose down-sampling ratios are 8, 16, 32, 64, 128, respectively.

Each location on the FPN's feature maps P_i either is associated with an instance, thus being a positive sample, or is considered a negative sample. The associated instance for each location are determined as follows. Let us consider the feature maps $P_i \in \mathbb{R}^{H \times W \times C}$ and let s be its down-sampling ratio. As shown in previous works [12, 30, 34], a location (x, y) on the feature maps can be mapped back onto the input image as $(xs + \lfloor \frac{s}{2} \rfloor, ys + \lfloor \frac{s}{2} \rfloor)$. If the mapped location falls in the center region of an instance, the location is considered to be responsible for the instance. Any location outside the center regions is labeled as a negative sample. The center region is defined by the box $(c_x - rs, c_y - rs, c_x + rs, c_y + rs)$, where (c_x, c_y) denotes the pseudo-box (minimum enclosing rectangles of the keypoints) center of the instance, s is the down-sampling ratio of P_i and r is a constant being 1.5 as in FCOS [34].

As shown in Figure 3, on each feature level of the FPN, some functional heads (in the dashed box) are applied to make instance-related predictions. For example, the classification head predicts the class (i.e., person or not person) of the instance associated with the location. Note that the parameters of these heads are shared between FPN levels.

3.2 Instance-Aware Dynamic Networks

Dynamic KP-Nets. To predict the parameters $\theta_{x,y}$ of the KP-Net with respect to the location (x, y) of the input feature map, we concatenate all the parameters in each KP-Net (i.e., weights and biases) together as a C_f -D vector, where C_f is the total number of the parameters. The KP-Net is a very compact FCN architecture, which has three 1×1 convolutions, each having 8 channels and using ReLU as the activation function except for the last one. No normalization layer such as batch normalization [15] is adopted here. The last layer has K (e.g., $K = 17$ in COCO [23] dataset) output channels and generates the final keypoint map for the instance. In particular, the KP-Net has 313 parameters in total, which consists of conv1 $((8+2) \times 8+8)$, conv2 $(8 \times 8+8)$ and conv3 $(8 \times 17+17)$. As mentioned before, the dynamically generated KP-Net contains

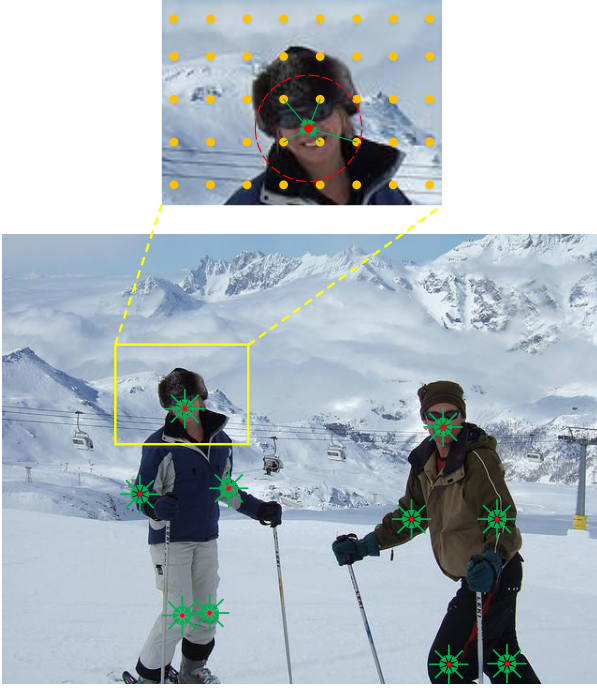


Figure 4: Illustration of disk offset estimation. In the top-most cropped image, orange dots represent feature points while the dotted circle represents the disk region corresponding to the nose. Each position within the disk predicts an offset vector (i.e., green arrow), which is utilized to improve the keypoint localization accuracy. We only draw the keypoints of nose, left_elbow, right_elbow, left_knee, right_knee for clarity.

information about the instance at the location. Thus, it will ideally only fire on the pixels of the instance’s keypoints, as shown in Figure 1.

Shared Inputs. As shown in Figure 3, there is a keypoint feature branch that provides the feature map F_{kp} for the final pose estimation. The keypoint feature branch is connected to FPN level P_3 with a down-sampling ratio of 8. It has four 3×3 convolutions with 128 channels before the last layer. Afterwards, in order to reduce the number of parameters in the KP-Net, the last layer of the keypoint feature branch reduces the number of channels from 128 to 8. Thus, the number of channels of F_{kp} is equal to 8 (i.e., $C_{kp} = 8$). Moreover, F_{kp} is combined with a map of the coordinates $R_{x,y} \in \mathbb{R}^{\frac{H}{s} \times \frac{W}{s} \times 2}$, which are relative coordinates from all the locations on F_{kp} to the location (x, y) (i.e., where the parameters $\theta_{x,y}$ are generated). Then, the combination $\tilde{F}_{x,y} \in \mathbb{R}^{\frac{H}{s} \times \frac{W}{s} \times (C_{kp}+2)}$ is sent to the KP-Nets to predict the keypoint map, which is omitted in Figure 3 for simplicity. The relative coordinate map can provide a strong cue for distinguishing different instances.

Optimization. The loss function of the instance-aware KP-Nets module can be formulated as:

$$L_{kpf}(\{\theta_{x,y}\}) = \frac{1}{N_{pos}} \sum_{x,y} \mathbb{1}_{\{c_{x,y}^* > 0\}} L_{ce}(FCN(\tilde{F}_{x,y}; \theta_{x,y}), M_{x,y}^*), \quad (4)$$

where $c_{x,y}^*$ is the classification label of location (x, y) , which is 1 if the location is associated with an instance and is 0 for indicating background. N_{pos} is the number of locations where $c_{x,y}^* > 0$. $\mathbb{1}_{\{c_{x,y}^* > 0\}}$ is the indicator function, being 1 if $c_{x,y}^* > 0$ and 0 otherwise. $\theta_{x,y}$ is the parameters of the KP-Net at location (x, y) . As described before, $\tilde{F}_{x,y}$ is the combination of the keypoint feature F_{kp} and the relative coordinate map $R_{x,y}$. FCN denotes the fully convolutional dynamic networks, which consists of the generated instance-aware parameters.

As mentioned before, the resolution of the predicted keypoint map is $\frac{1}{s}$ of the input image’s resolution. Thus, for each visible ground-truth keypoint of an instance, we compute a low-resolution equivalent $\hat{p} = (\lfloor \frac{x^*}{s} \rfloor, \lfloor \frac{y^*}{s} \rfloor)$. The training target is a one-hot $\frac{H}{s} \times \frac{W}{s}$ binary mask where only a *single* pixel at location \hat{p} is labeled as foreground. $M_{x,y}^* \in \{0, 1\}^{\frac{H}{s} \times \frac{W}{s} \times K}$ represents the one-hot masks of the person instance associated with location (x, y) . L_{ce} is the softmax cross-entropy loss, which encourages a single point to be detected. These operations are omitted in Equation (4) for clarification.

3.3 Disk Offset Estimation

Suppose that $M_i \in \mathbb{R}^{\frac{H}{s} \times \frac{W}{s} \times K}$ is the predicted keypoint map for the i th person. The location of maximal activation in the j th channel of M_i indicates the location of the j th keypoint of person i , which is defined as $\bar{P}_i^j = (\bar{x}_i^j, \bar{y}_i^j)$. We can get the final keypoint location by mapping back \bar{P}_i^j onto input image plane as $((\bar{x}_i^j + 0.5) \times s, (\bar{y}_i^j + 0.5) \times s)$. However, there is a discretization error in this naive position mapping due to the down-sampling operation. In order to compensate for the discretization error, we predict a instance-agnostic local offset $O \in \mathbb{R}^{\frac{H}{s} \times \frac{W}{s} \times 2K}$ for each category of keypoints.

As shown in Figure 3, the disk offset branch takes the FPN feature maps P_3 as input. Afterwards, three 3×3 conv layers are applied for the final disk offset prediction. There are $2K$ output channels in the offset prediction, indicating the displacements in both the horizontal and vertical directions. Let p be the 2-D position in the feature plane, and $\mathcal{D}_R = \{p : \|p - P_i^j\| \leq R\}$ be a disk of radius R centered around P_i^j , where P_i^j represents the 2-D position of the j th keypoint of the i th person. As illustrated in Figure 4, for each position p within the disk region \mathcal{D}_R , the 2-D offset vector which points from the image position x_j to keypoint P_i^j is generated. During training, we penalize the disk offset regression errors with the L_1 loss. The supervision is only performed in the disk region. During inference, the position of maximum response $(\bar{x}_i^j, \bar{y}_i^j)$ in the keypoint map is shifted by the corresponding offset vector $(\Delta x, \Delta y)$. Then the final result can be formulated as $((\bar{x}_i^j + \Delta x) \times s, (\bar{y}_i^j + \Delta y) \times s)$. This well-designed module can further improve pose estimation performance, as shown in our experiments.

Table 1: Ablation experiments on COCO minival. “Disk offset”: the predicted local offset for recovering the discretization error caused by the keypoint map stride. “Heatmap”: using heatmap to assist training.

	Disk offset	Heatmap	AP	AP ₅₀	AP ₇₅	AP _M	AP _L	AR	AR ₅₀	AR ₇₅
Our InsPose			60.3	85.4	65.5	55.0	68.4	68.6	91.0	73.7
Our InsPose	✓		62.1	86.0	67.5	57.6	69.1	70.2	91.4	75.3
Our InsPose	✓	✓	63.1	86.2	68.5	58.5	70.1	70.9	91.2	76.1

3.4 Training and Inference

Training and Loss Function. Given the fact that multi-task learning facilitates the training of models, we adopt a multi-person heatmap prediction as an auxiliary task, which is omitted in Figure 3 for simplicity. The heatmap prediction task takes as input the FPN feature maps P_3 . Afterwards, two 3×3 convolutions with channel being 256 are applied here. Finally, another 3×3 convolution layer with the output channel being K is appended for the final heatmap prediction, where K is the number of keypoint categories in the dataset. As shown in the following experiments, this joint learning procedure can boost the performance of our model. Note that the heatmap-based task is only used for auxiliary supervision during training and is removed when testing.

Formally, the overall loss function of InsPose can be formulated as:

$$L = L_{cls} + L_{kpf} + L_{do} + L_{hm} \quad (5)$$

where L_{cls} is the focal loss function [22] for the classification branch, L_{kpf} is the loss of instance-aware KP-Nets module as defined in Equation (4), L_{do} is L1 loss for disk offset regression, L_{hm} is a variant of focal loss [19] for the auxiliary heatmap branch.

Inference. The inference of InsPose is simple and straightforward. Given an input image, we forward it through the network to obtain the outputs including classification confidence $p_{x,y}$ and the generated parameters $\theta_{x,y}$ of the KP-Net at location (x,y) . We first use a confidence threshold of 0.1 to filter out predictions with low confidence. Then we select the top N (i.e., $N = 500$) scoring person instances and their corresponding parameters. Then the N groups of pose estimation results can be obtained through Equations (2) and (3). At last, We do non-maximum suppression (NMS) using the minimum enclosing rectangles of estimated keypoints of the instances. The top 100 instance keypoints in each image are kept for evaluation.

It is worth noting that our framework can conveniently be adapted to simultaneous bounding-box and keypoint detection by attaching a bounding-box head, which shares the preceding convolutions of the parameter generating branch for KP-Nets.

4 EXPERIMENTS

We evaluate our proposed InsPose on the human keypoint detection task of the large-scale COCO benchmark dataset [23]. The dataset contains more than 250K instances where each person has 17 annotated keypoints. Following the common practice [11, 33, 38], we use the COCO trainval35k split (57K images) for training and minival split (5K images) as validation for our ablation study. We report our main results on the test-dev split (20K images). The performance is computed with Average Precision (AP) based on Object Keypoint Similarity (OKS).

Implementation Details: Unless specified, ablation studies are conducted with ResNet-50 [13] and FPN [21]. The models are trained with stochastic gradient descent (SGD) with a minibatch of 16 images. The initial learning rate is set to 0.01. Weight decay and momentum are set as 0.0001 and 0.9, respectively. Specifically, the model is trained for 36 epochs and the initial learning rate is divided by 10 at epoch 27 and 33 in ablation experiments. For the main results on test-dev split, we train the models for 100 epochs and the initial learning rate is divided by 10 at epoch 75 and 90. We initialize our backbone networks with the weights pre-trained on ImageNet [8]. For the newly added layers, we initialize them as in [22]. When training, the images are resized to have their shorter sides in [640, 800] and their longer sides less or equal to 1333, and then they are randomly horizontally flipped with the probability of 0.5. No extra data augmentation like rotation [26] or random cropping [33] is used during training. When testing, the input images are resized to have their shorter sides being 800 and their longer sides less or equal to 1333.

4.1 Ablation Experiments

Baseline. First, we conduct the experiments through employing instance-aware dynamic networks to produce keypoint maps where the maximal activation of each channel is chosen as the keypoint. As shown in Table 1 (1st row), the naive framework can obtain competitive performance (60.3% in AP^{kp}). As shown in Figure 3, we apply the local offset predicted by the disk offset branch to recover the discretization error of keypoint maps. As shown in Table 1 (2nd row), the performance is improved from 60.3% to 62.1% in AP^{kp}, which demonstrate the effectiveness of disk offset branch. Therefore, in the sequel, we will use the disk offset branch for all the following experiments. By jointly learning with a heatmap prediction task, the performance of our model can be further improved from 62.1% to 63.1%, as shown in Table 1 (3rd row). Note that the heatmap prediction is only used during training to provide the multi-task regularization and is pruned during inference. We show some visualization results of InsPose in Figure 2.

Architecture of KP-Net. In this section, we discuss the architecture of the KP-Nets in InsPose. Our baseline is the KP-Net of three 1×1 convolutions with 8 channels considering the high capacity of conditional convolutions, which contains a total of 313 parameters. As shown in Table 2 (3rd row), it achieves 63.1% in AP^{kp}. Then, we conduct experiments by varying the depth of the KP-Net. As shown in Table 2, the depth being 1 achieves inferior performance as in this case the KP-Net is actually a linear mapping, which has overly weak capacity. With the depth increases, the performance is improved gradually due to the higher capacity of the KP-Net. However, the performance drops slightly when the

Table 2: Ablation experiments on COCO minival with different depth of KP-Nets. “depth”: the number of conv. layers in the KP-Nets.

depth	AP	AP ₅₀	AP ₇₅	AP _M	AP _L
1	54.7	81.1	57.4	50.5	62.2
2	62.4	85.9	67.9	58.0	69.2
3	63.1	86.2	68.5	58.5	70.1
4	61.7	85.9	67.2	57.1	68.7

Table 3: Ablation experiments on COCO minival with different resolution of keypoint score maps and disk offset predictions. “res. ratio”: the resolution ratio of the above two predictions to the input image.

res. ratio	AP	AP ₅₀	AP ₇₅	AP _M	AP _L
1/16	62.6	85.8	68.2	57.2	70.5
1/8	63.1	86.2	68.5	58.5	70.1
1/4	62.0	83.9	67.5	57.8	69.1
1/2	45.4	73.6	47.0	39.1	54.7

depth increases further mainly due to the reason that it is harder to optimize more dynamic parameters.

Resolution of Keypoint Maps and Disk Offset Predictions.

Intuitively, the resolution of the above two predictions is of great importance to the final performance due to pose estimation being a position-sensitive task. We investigate this in the experiment. As shown in Figure 3, the resolution of the origin keypoint score maps and disk offset predictions is same as the resolution of P3 features, which is $\frac{1}{8}$ of the input image resolution. As shown in Table 3, our baseline model (2nd row in the table) achieves 63.1% in AP^{kp}. If both of the two predictions is downsampled to the $\frac{1}{16}$ of the input image resolution (1st row in the table), the performance drops slightly (from 63.1% to 62.6%). In particular, AP_M drops remarkably by 1.3% (from 58.5% to 57.2%), which indicating that low-resolution predictions harms the performance of small-scale persons. Additionally, upsampling both of the predictions by a factor of 2 and 4 (using bilinear interpolation), the performance is degraded by 1.1% and 16.6, respectively. This is probably due to the relatively low-quality annotations of keypoints, which causes a growing negative impact on the training of the model as the output resolution increases.

Combining with Bounding Box Detection. By simply attaching a bounding-box regression head, we can simultaneously detect bounding-boxes and keypoints of the instances. When testing, NMS is applied to the detected bounding-boxes instead of the minimum enclosing rectangles of keypoints. Here we confirm it by the experiment. As shown in Table 4, our framework can achieve a reasonable person detection performance, which is competitive with the Faster R-CNN detector in Mask R-CNN [11] (52.5% vs. 50.7%). Meanwhile, the keypoint performance drops a little due to different positive/negative label assignments between the detection-boxes and pseudo-boxes at training phase.

Table 4: Ablation experiments on COCO minival for InsPose with person bounding-box detection. The proposed framework can achieve reasonable person detection results (52.5% in box AP). As a reference, the Faster R-CNN person detector in Mask R-CNN [11] achieves 50.7% in box AP.

w/ bbox	AP ^{bb}	AP ^{kp}	AP ₅₀ ^{kp}	AP ₇₅ ^{kp}	AP _M ^{kp}	AP _L ^{kp}
-	-	63.1	86.2	68.5	58.5	70.1
✓	52.5	62.5	86.2	68.1	58.3	70.3

4.2 Comparisons with State-of-the-art Methods

In this section, we evaluate the proposed single-stage multi-person pose estimator on MS-COCO test-dev and compare it with other state-of-the-art methods. As shown in Table 5, without any bells and whistles (e.g., multi-scale and flipping testing, the refining in [3, 25], and any other tricks), the proposed framework achieves 65.4% and 66.3% in AP^{kp} on COCO test-dev split, with ResNet-50 and ResNet-101 as the backbone, respectively. With multi-scale testing, our framework can reach 71.0% in AP^{kp} with HRNet-w32.

Compared to Single-stage Methods: Our method significantly outperforms existing single-stage methods, such as DirectPose [33], CenterNet [42], SPM [26] and Point-Set Anchors [38]. The performance of our method is +3.2% and +3.0% higher as compared to DirectPose [33] with ResNet-50 and ResNet-101, respectively. InsPose with HRNet-w32 even outperforms the latest single-stage pose estimator Point-Set Anchors [38] with HRNet-w48, 71.0% vs. 68.7% in AP^{kp}. Note that our model is anchor-free and Point-Set Anchors need 27 carefully chosen pose anchors per location.

Compared to Bottom-up Methods: Our method outperforms the state-of-the-art bottom-up methods, such as CMU-Pose [3], AE [25], PersonLab [27], PifPaf [18], HigherHRNet [6] and the latest DGCN [29]. With single-scale testing, it achieves significant improvement over HigherHRNet, 69.3% vs. 66.4% in AP^{kp}, using the same backbone HRNet-w32. Besides that, our performance with HRNet-w32 is higher than DGCN [29] with ResNet-152, 69.3% vs. 67.4% in AP^{kp}.

Compared to Top-down Methods: With the same backbone ResNet-50, the proposed method outperforms previous strong baseline Mask R-CNN (65.4% vs. 62.7% in AP^{kp}). Our model is still behind other top-down methods, since they mitigate the scale variance of persons by cropping and resizing the detected person into the same scale. As noted before, two-stage methods take an additional person detector and employ a single person pose estimator to each cropped image, resulting in high computation overhead. In contrast, our method is much simpler and faster since we eliminate the redundant person detector.

Inference Time Comparison: We measure the inference time of all variants of our method and other methods on the same hardware if possible. As shown in Table 5, InsPose with HRNet-w32 can infer faster than Point-Set Anchors [38] (0.15s vs. 0.27s per image). And it also runs significantly faster than state-of-the-art top-down methods, such as HRNet [32] (>2.34s per image) and RSN [2] (>3.06s per image). Note that the time of additional person detector used in HRNet and RSN is not included here. Moreover, we

Table 5: Comparison with state-of-the-art methods on MS COCO test-dev dataset. * and † denote multi-scale testing and using additional refinement, respectively. We compare the average inference time per image of our methods with other state-of-the-art single-stage and two-stage methods. The time is counted with single-scale testing on a single NVIDIA TITAN X GPU.

Method	Backbone	AP	AP ₅₀	AP ₇₅	AP _M	AP _L	Times[s]
Top-down Methods							
Mask-RCNN [11]	ResNet-50	62.7	87.0	68.4	57.4	71.1	0.08
CPN [5]	ResNet-Inception	72.1	91.4	80.0	68.7	77.2	> 0.65
HRNet [32]	HRNet-w32	74.9	92.5	82.8	71.3	80.9	> 2.34
ECSI [31]	ResNet-152	74.3	91.8	81.9	70.7	80.2	-
RSN [2]	2 × RSN-50	75.5	93.6	84.0	73.0	79.6	> 3.06
Bottom-up Methods							
CMU-Pose*† [3]	3CM-3PAF (102)	61.8	84.9	67.5	57.1	68.2	-
AE*† [25]	Hourglass-4 stacked	65.5	87.1	71.4	61.3	71.5	0.52
PersonLab [27]	ResNet-101	65.5	87.1	71.4	61.3	71.5	-
PifPaf [18]	ResNet-152	66.7	-	-	62.4	72.9	0.26
HigherHRNet [6]	HRNet-w32	66.4	87.5	72.8	61.2	74.2	0.60
DGCN [29]	ResNet-152	67.4	88.0	74.4	63.6	73.0	> 0.26
Single-stage Methods							
DirectPose [33]	ResNet-50	62.2	86.4	68.2	56.7	69.8	-
DirectPose [33]	ResNet-101	63.3	86.7	69.4	57.8	71.2	-
CenterNet [42]	Hourglass-104	63.0	86.8	69.6	58.9	70.4	0.16
SPM*† [26]	Hourglass-8 stacked	66.9	88.5	72.9	62.6	73.1	-
Point-Set Anchors* [38]	HRNet-w48	68.7	89.9	76.3	64.8	75.3	0.27
Our InsPose	ResNet-50	65.4	88.9	71.7	60.2	72.7	0.08
Our InsPose*	ResNet-50	67.1	89.7	74.0	62.6	73.8	-
Our InsPose	ResNet-101	66.3	89.2	73.0	61.2	73.9	0.10
Our InsPose*	ResNet-101	67.8	90.3	74.9	64.3	73.4	-
Our InsPose	HRNet-w32	69.3	90.3	76.0	64.8	76.1	0.15
Our InsPose*	HRNet-w32	71.0	91.3	78.0	67.5	76.5	-

notice that the grouping post-processing in the bottom-up method HigherHRNet [6] (0.60s per image) is time-consuming and results in inferior speed compared to InsPose. Overall, InsPose makes a good trade-off between the accuracy and efficiency, benefiting from its simple single-stage framework.

5 CONCLUSION

In this paper, we present a single-stage multi-person pose estimation method, termed InsPose. It directly maps a raw input image to the desired instance-aware poses, get rid of the need for the grouping post-processing in bottom-up methods or the bounding-box detection in top-down approaches. Specifically, we propose an instance-aware module to adaptively adjust (part of) the network parameters for each instance. Our method can significantly increase the capacity and adaptive-ability of the network for recognizing various poses, while maintaining a compact end-to-end trainable pipeline. We also propose a disk offset branch to recover the discretization error due to down-sampling, boosting the keypoint detection performance further. We conduct extensive experiments on the MS-COCO dataset where our method achieves significant improvement over existing single-stage methods and performs

comparably with state-of-the-art two-stage methods in terms of accuracy and efficiency.

REFERENCES

- [1] Qian Bao, Wu Liu, Jun Hong, Lingyu Duan, and Tao Mei. 2020. Pose-native Network Architecture Search for Multi-person Human Pose Estimation. In *ACM International Conference on Multimedia*. ACM, 592–600.
- [2] Yuanhao Cai, Zhicheng Wang, Zhengxiong Luo, Binyi Yin, Angang Du, Haoqian Wang, Xiangyu Zhang, Xinyu Zhou, Erjin Zhou, and Jian Sun. 2020. Learning delicate local representations for multi-person pose estimation. In *European Conference on Computer Vision*. Springer, 455–472.
- [3] Zhe Cao, Tomas Simon, Shih-En Wei, and Yaser Sheikh. 2017. Realtime multi-person 2d pose estimation using part affinity fields. In *Proceedings of the IEEE conference on computer vision and pattern recognition*. 7291–7299.
- [4] Yinpeng Chen, Xiyang Dai, Mengchen Liu, Dongdong Chen, Lu Yuan, and Zicheng Liu. 2020. Dynamic Convolution: Attention Over Convolution Kernels. In *Proceedings of the IEEE/CVF Conference on Computer Vision and Pattern Recognition (CVPR)*.
- [5] Yilun Chen, Zhicheng Wang, Yuxiang Peng, Zhiqiang Zhang, Gang Yu, and Jian Sun. 2018. Cascaded pyramid network for multi-person pose estimation. In *Proceedings of the IEEE conference on computer vision and pattern recognition*. 7103–7112.
- [6] Bowen Cheng, Bin Xiao, Jingdong Wang, Honghui Shi, Thomas S Huang, and Lei Zhang. 2020. Higherhrnet: Scale-aware representation learning for bottom-up human pose estimation. In *Proceedings of the IEEE/CVF Conference on Computer Vision and Pattern Recognition*. 5386–5395.
- [7] Yan Dai, Xuanhan Wang, Lianli Gao, Jingkuan Song, and Heng Tao Shen. 2021. RSGNet: Relation based Skeleton Graph Network for Crowded Scenes Pose

- Estimation. (2021).
- [8] Jia Deng, Wei Dong, Richard Socher, Li-Jia Li, Kai Li, and Li Fei-Fei. 2009. Imagenet: A large-scale hierarchical image database. In *2009 IEEE conference on computer vision and pattern recognition*. Ieee, 248–255.
 - [9] Misha Denil, Babak Shakhbibi, Laurent Dinh, Marc’Aurelio Ranzato, and Nando de Freitas. 2013. Predicting Parameters in Deep Learning. In *NIPS*. 2148–2156.
 - [10] Hao-Shu Fang, Shuqin Xie, Yu-Wing Tai, and Cewu Lu. 2017. Rmpe: Regional multi-person pose estimation. In *Proceedings of the IEEE International Conference on Computer Vision*. 2334–2343.
 - [11] Kaiming He, Georgia Gkioxari, Piotr Dollár, and Ross Girshick. 2017. Mask r-cnn. In *Proceedings of the IEEE international conference on computer vision*. 2961–2969.
 - [12] Kaiming He, Xiangyu Zhang, Shaoqing Ren, and Jian Sun. 2015. Spatial pyramid pooling in deep convolutional networks for visual recognition. *IEEE transactions on pattern analysis and machine intelligence* 37, 9 (2015), 1904–1916.
 - [13] Kaiming He, Xiangyu Zhang, Shaoqing Ren, and Jian Sun. 2016. Deep residual learning for image recognition. In *Proceedings of the IEEE conference on computer vision and pattern recognition*. 770–778.
 - [14] Eldar Insafutdinov, Leonid Pishchulin, Bjoern Andres, Mykhaylo Andriluka, and Bernt Schiele. 2016. Deepcrut: A deeper, stronger, and faster multi-person pose estimation model. In *European Conference on Computer Vision*. Springer, 34–50.
 - [15] Sergey Ioffe and Christian Szegedy. 2015. Batch normalization: Accelerating deep network training by reducing internal covariate shift. In *International conference on machine learning*. PMLR, 448–456.
 - [16] Xu Jia, Bert De Brabandere, Tinne Tuytelaars, and Luc Van Gool. 2016. Dynamic filter networks. In *NIPS*.
 - [17] Chenru Jiang, Kaizhu Huang, Shufei Zhang, Xinheng Wang, and Jimin Xiao. 2020. Pay Attention Selectively and Comprehensively: Pyramid Gating Network for Human Pose Estimation without Pre-training. In *ACM International Conference on Multimedia*. ACM, 2364–2371.
 - [18] Sven Kreiss, Lorenzo Bertoni, and Alexandre Alahi. 2019. Pifpaf: Composite fields for human pose estimation. In *Proceedings of the IEEE/CVF Conference on Computer Vision and Pattern Recognition*. 11977–11986.
 - [19] Hei Law and Jia Deng. 2018. Cornernet: Detecting objects as paired keypoints. In *Proceedings of the European conference on computer vision (ECCV)*. 734–750.
 - [20] Wei Li, Xiataian Zhu, and Shaogang Gong. 2018. Harmonious attention network for person re-identification. In *Proceedings of the IEEE conference on computer vision and pattern recognition*. 2285–2294.
 - [21] Tsung-Yi Lin, Piotr Dollár, Ross Girshick, Kaiming He, Bharath Hariharan, and Serge Belongie. 2017. Feature pyramid networks for object detection. In *Proceedings of the IEEE conference on computer vision and pattern recognition*. 2117–2125.
 - [22] Tsung-Yi Lin, Priya Goyal, Ross Girshick, Kaiming He, and Piotr Dollár. 2017. Focal loss for dense object detection. In *Proceedings of the IEEE international conference on computer vision*. 2980–2988.
 - [23] Tsung-Yi Lin, Michael Maire, Serge Belongie, James Hays, Pietro Perona, Deva Ramanan, Piotr Dollár, and C Lawrence Zitnick. 2014. Microsoft coco: Common objects in context. In *European conference on computer vision*. Springer, 740–755.
 - [24] Weian Mao, Zhi Tian, Xinlong Wang, and Chunhua Shen. 2021. FCPose: Fully Convolutional Multi-Person Pose Estimation With Dynamic Instance-Aware Convolutions. In *Proceedings of the IEEE/CVF Conference on Computer Vision and Pattern Recognition (CVPR)*. 9034–9043.
 - [25] Alejandro Newell, Zhiao Huang, and Jia Deng. 2016. Associative embedding: End-to-end learning for joint detection and grouping. *arXiv preprint arXiv:1611.05424* (2016).
 - [26] Xuecheng Nie, Jiashi Feng, Jianfeng Zhang, and Shuicheng Yan. 2019. Single-stage multi-person pose machines. In *Proceedings of the IEEE/CVF International Conference on Computer Vision*. 6951–6960.
 - [27] George Papandreou, Tyler Zhu, Liang-Chieh Chen, Spyros Gidaris, Jonathan Tompson, and Kevin Murphy. 2018. Personlab: Person pose estimation and instance segmentation with a bottom-up, part-based, geometric embedding model. In *Proceedings of the European Conference on Computer Vision (ECCV)*. 269–286.
 - [28] Leonid Pishchulin, Eldar Insafutdinov, Siyu Tang, Bjoern Andres, Mykhaylo Andriluka, Peter V Gehler, and Bernt Schiele. 2016. Deepcut: Joint subset partition and labeling for multi person pose estimation. In *Proceedings of the IEEE conference on computer vision and pattern recognition*. 4929–4937.
 - [29] Zhongwei Qiu, Kai Qiu, Jianlong Fu, and Dongmei Fu. 2020. Dgcn: Dynamic graph convolutional network for efficient multi-person pose estimation. In *Proceedings of the AAAI Conference on Artificial Intelligence*, Vol. 34. 11924–11931.
 - [30] Shaoqing Ren, Kaiming He, Ross Girshick, and Jian Sun. 2015. Faster r-cnn: Towards real-time object detection with region proposal networks. *arXiv preprint arXiv:1506.01497* (2015).
 - [31] Kai Su, Dongdong Yu, Zhenqi Xu, Xin Geng, and Changhu Wang. 2019. Multi-person pose estimation with enhanced channel-wise and spatial information. In *Proceedings of the IEEE/CVF Conference on Computer Vision and Pattern Recognition*. 5674–5682.
 - [32] Ke Sun, Bin Xiao, Dong Liu, and Jingdong Wang. 2019. Deep high-resolution representation learning for human pose estimation. In *Proceedings of the IEEE/CVF Conference on Computer Vision and Pattern Recognition*. 5693–5703.
 - [33] Zhi Tian, Hao Chen, and Chunhua Shen. 2019. Directpose: Direct end-to-end multi-person pose estimation. *arXiv preprint arXiv:1911.07451* (2019).
 - [34] Zhi Tian, Chunhua Shen, Hao Chen, and Tong He. 2019. Fcos: Fully convolutional one-stage object detection. In *Proceedings of the IEEE/CVF International Conference on Computer Vision*. 9627–9636.
 - [35] Chunyu Wang, Yizhou Wang, and Alan L Yuille. 2013. An approach to pose-based action recognition. In *Proceedings of the IEEE conference on computer vision and pattern recognition*. 915–922.
 - [36] Jianbo Wang, Kai Qiu, Houwen Peng, Jianlong Fu, and Jianke Zhu. 2019. AI Coach: Deep Human Pose Estimation and Analysis for Personalized Athletic Training Assistance. In *ACM International Conference on Multimedia*. ACM, 374–382.
 - [37] Pichao Wang, Wanqing Li, Philip Ogunbona, Jun Wan, and Sergio Escalera. 2018. RGB-D-based human motion recognition with deep learning: A survey. *Computer Vision and Image Understanding* 171 (2018), 118–139.
 - [38] Fangyun Wei, Xiao Sun, Hongyang Li, Jingdong Wang, and Stephen Lin. 2020. Point-set anchors for object detection, instance segmentation and pose estimation. In *European Conference on Computer Vision*. Springer, 527–544.
 - [39] Bin Xiao, Haiping Wu, and Yichen Wei. 2018. Simple baselines for human pose estimation and tracking. In *Proceedings of the European conference on computer vision (ECCV)*. 466–481.
 - [40] Brandon Yang, Gabriel Bender, Quoc V Le, and Jiquan Ngiam. 2019. Condconv: Conditionally parameterized convolutions for efficient inference. *arXiv preprint arXiv:1904.04971* (2019).
 - [41] Shifeng Zhang, Cheng Chi, Yongqiang Yao, Zhen Lei, and Stan Z Li. 2020. Bridging the gap between anchor-based and anchor-free detection via adaptive training sample selection. In *Proceedings of the IEEE/CVF Conference on Computer Vision and Pattern Recognition*. 9759–9768.
 - [42] Xingyi Zhou, Dequan Wang, and Philipp Krähenbühl. 2019. Objects as points. *arXiv preprint arXiv:1904.07850* (2019).
 - [43] Xiaojun Zhu, Qun Li, and Guihai Chen. 2013. APT: Accurate outdoor pedestrian tracking with smartphones. In *2013 Proceedings IEEE INFOCOM*. IEEE, 2508–2516.